Med Biol Eng Comput (2010) 48:1281–1291
DOI 10.1007/s11517-010-0650-x

ORIGINAL ARTICLE

Enhancement of the ultrasound images by modified anisotropic diffusion method

Deepti Mittal · Vinod Kumar · Suresh Chandra Saxena · Niranjan Khandelwal · Naveen Kalra

Received: 26 August 2009 / Accepted: 2 June 2010 / Published online: 24 June 2010

Abstract Speckle is a primary factor which degrades the contrast resolution and masks the meaningful texture information present in an ultrasound image. Its presence severely hampers the interpretation and analysis of ultrasound images. When speckle reduction technique is applied for visual enhancement of ultrasound images, it is to be kept in mind that blurring associated with speckle reduction should be less and fine details are properly enhanced. With these points in consideration, the modified speckle reduction anisotropic diffusion (MSRAD) method is proposed in the present study to improve the visual quality of the ultrasound images. In the proposed MSRAD method, the four neighboring pixel template in speckle reduction anisotropic diffusion (SRAD) method of Yu and Acton (IEEE Trans Image Process 11:1260–1270, 2002) have been replaced by a new template of larger number of neighboring pixels to calculate the diffusion term. To enhance visual quality of ultrasound images, nonquadratic regularization (Yu and Yadegar, Proceedings of the IEEE international conference on image processing, 2006) is incorporated with MSRAD method and accordingly changes in parameter settings have been made. The performance of MSRAD method was evaluated using clinical ultrasound images, interpretation by the medical experts and results of MSRAD method by subjective and objective criteria.

D. Mittal (✉) · V. Kumar · S. C. Saxena
Department of Electrical Engineering, Indian Institute of Technology Roorkee, Roorkee 247667, India
e-mail: deeptimit@gmail.com

N. Khandelwal · N. Kalra
Department of Radiodiagnosis, Postgraduate Institute of Medical Education and Research, Chandigarh 160012, India

Keywords Enhancement · Speckle · Ultrasound · MSRAD · SRAD

1 Introduction

In the past several decades, ultrasonography has become a very popular tool for imaging physiological systems in the body. Ultrasonography is the second most performed procedure, right after X-ray imaging: because of its real-time imaging, nonradioactive, noninvasive, and inexpensive nature. The accurate interpretation of ultrasound image is hampered by two signal processing roadblocks. First, subresolution scatterers lead to image speckle that plagues imaging applications by obscuring the underlying tissue properties. Second, the imaging system itself has a point spread function that creates blurring of image features [4]. Both these factors degrade the image quality and thus cause a problem for medical practitioner to discriminate fine details of the image during diagnostic examinations. As a result, image processing for reducing the speckle noise and blurring is a critical pre-processing step. However, speckle is not a genuine noise because its texture often carries certain information about the image being viewed [34] and it can be useful for detecting and differentiating different type of lesions. Sometimes, clinicians are afraid that speckle reduction process may suppress the important details of ultrasound image, so speckle reduction should be designed such that it smoothens the image in a controlled fashion without significant loss of information. Such technique developed in consultation with doctors enhances the details of ultrasound image and an enhanced ultrasound image improves the doctor's diagnosis. It is an area of prime concern for researchers and still there is a need of a method that can sufficiently remove the speckle, retain

sharp features of the image from the blurred one, and simultaneously maintain and enhance its clinically useful features.

Speckle reduction techniques are primarily categorized as compounding (image averaging) and postacquisition (image filtering) techniques [1]. Filtering techniques have the advantage that they are not affected by the acquisition process. Filtering techniques can be classified as single scale spatial filtering (linear, nonlinear, adaptive methods, etc.), multiscale spatial filtering (anisotropic diffusion-based methods) and several multiscale methods in other domain (pyramid-based, wavelet, curvelet, counterlet, etc.). Linear spatial filters like mean filters degrade sharp details such as lines or edges [25, 36]. Nonlinear filters, e.g., weighted median filtering [10] retains edges but it results in a loss of resolution by suppressing fine details. Another approach is adaptive filtering [11, 12, 19, 20], which entail a tradeoff between smoothing efficiency and preservation of discontinuities. Several researchers [2, 3, 6, 7, 9, 13, 16–18, 31, 35, 37, 38, 41] proposed anisotropic diffusion methods based on the original study of Perona and Malik [24], where the anisotropic diffusion equation provides a technique for selective image smoothing. The development of research for anisotropic diffusion via the partial differential equation has taken place in such a way that important structures in the images remain preserved. Apart from anisotropic diffusion methods, several multi-scale approaches [8, 14, 15, 26, 28, 30, 32, 42, 45] were also proposed to reduce speckle in ultrasound images. Most of the recent studies [22, 23, 27, 43–45] on speckle reduction techniques are based on fusion of anisotropic diffusion and multiscale techniques. These techniques are more suited for segmentation purposes rather than feature extraction and visual diagnosis from the real ultrasound images due to the complexity of speckle statistics involved in feature extraction and visual diagnosis. When speckle reduction is applied as a preprocessing step for segmentation or registration, speckle can be considered noise without any differentiation. When speckle reduction technique is applied for feature extraction and visual diagnosis, texture recovery is considered as a desired feature of filtering. Clinicians prefer an original image to a despeckled image for the diagnosis of liver and kidney problems, because the original image contains more diagnostic information. From this point of view, speckle reduction method should be a balance between speckle suppression and feature preservation and despeckled image should be a complement to the original image, not a replacement.

Speckle reducing anisotropic diffusion (SRAD) proposed by Yu and Acton [38] is an approach to alleviate the effect of speckle. This method has adopted Lee's and Frost's adaptive filtering idea into anisotropic diffusion algorithm by exploiting the instantaneous coefficient of variation (ICOV). ICOV serves as the edge or high-contrast feature detector in speckled image. SRAD excels in terms of mean preservation, variance reduction, and edge localization in the presence of speckle noise over adaptive filter algorithms and it also shows a very good performance with different levels of speckle. Although it makes fine details to be more visible in the images, it still has limitation in retaining subtle features such as small cysts and lesions in ultrasound images because of its blurring and eradicating nature. In the present study, SRAD is modified to preserve the texture of ultrasound images by the limited speckle reduction with reduced blurring and in addition, it is combined with the regularizing method [40] for overall visual quality enhancement of ultrasound images.

2 Methods

2.1 Background

Anisotropic diffusion is widely used as a *multi-scale nonlinear* image processing technique that offers a good compromise between noise removal and edge preservation. The Gaussian representation introduces a scale dimension by convolving the original image with a Gaussian kernel. This idea is applied in diffusion equation for multi-scale approach of image structure analysis. Perona and Malik [24] developed a multiscale smoothing and edge detection method by incorporating the image gradient into image diffusion-based filtering method to produce adaptive edge-preserving image filters. Their approach is useful in the case of additive noise, but not with speckle that is a multiplicative locally correlated noise.

Adaptive filters that aimed to reduce speckle, such as proposed by Lee [20] and Kuan [19], were based on the minimum mean square error (MMSE) approach, where the regions with low and constant variance are identified as the areas for noise reduction and the regions with high variance are identified as edges. Mean filter is applied for noise reduction in the homogeneous areas, whereas the areas containing edges are passed through the identity filter. The balance between these two filters is achieved by the *coefficient* of *variation* representing the local statistics. Yu and Acton [38] applied the coefficient of variation to anisotropic diffusion and proposed the speckle reducing anisotropic diffusion (SRAD) method. This method allows the generation of an image scale space by combining the advantages of the above two approaches.

2.1.1 SRAD method

SRAD method is briefed, by first representing the discrete form of anisotropic diffusion equation, as

$$I_{i,j}^{t+\Delta t} = I_{i,j}^{t} + \frac{\Delta t}{|\eta_{i,j}|}\sum_{p\in\eta_{i,j}} c\left(\left(\nabla I_{i,j}^{t}\right)_p\right)\cdot\left(\left(\nabla I_{i,j}^{t}\right)_p\right) \quad (1)$$

where I_{ij}^{t} is the discretely sampled images with pixel position(i, j), $\eta_{i,j}$ is spatial neighborhood of the pixel(i, j), $|\eta_{i,j}|$ is the number of pixels in this neighborhood window and Δt is the time step size. Yu and Acton in [38] have substituted the gradient-driven diffusion coefficient $c((\nabla I_{ij}^{t})_p)$ with the *coefficient of variation* of the adaptive filtering approach and they called it an *instantaneous coefficient of variation* (ICOV). The diffusion equation can be rewritten as

$$I_{i,j}^{t+\Delta t} = I_{i,j}^{t} + \frac{\Delta t}{|\eta_{i,j}|}\sum_{p\in\eta_{i,j}} c\left(\left(\mathrm{ICOV}_{i,j}^{t}\right)_p\right)\cdot\left(\left(\nabla I_{i,j}^{t}\right)_p\right) \quad (2)$$

The diffusion coefficient $c(\cdot)$ should be any bounded non-negative decreasing function that is given in [38] as

$$c(\mathrm{ICOV}) = \exp\left(-\frac{\left(\mathrm{ICOV}^2 - \mathrm{ICOV}_0^2\right)}{\left(\mathrm{ICOV}_0^2\left(1+\mathrm{ICOV}_0^2\right)\right)}\right) \quad (3)$$

$$c(\mathrm{ICOV}) = \frac{1}{1+\frac{\left(\mathrm{ICOV}^2-\mathrm{ICOV}_0^2\right)}{\left(\mathrm{ICOV}_0^2\left(1+\mathrm{ICOV}_0^2\right)\right)}} \quad (4)$$

where $\mathrm{ICOV}_0 \equiv \mathrm{ICOV}_0^t$ is a speckle scale function that effectively determines the amount of smoothing to be applied to the image. Speckle scale function is estimated iteratively by the intensity variance and mean over a homogeneous area. $\mathrm{ICOV} \equiv \mathrm{ICOV}_{ij}^{t}$, is obtained in terms of the discrete approximations to the derivatives of I, say ∇I and $\nabla^2 I$ in the neighborhood template and is expressed by the following expression in [40] as

$$\mathrm{ICOV} = \sqrt{\frac{\left|\left(\frac{1}{2}\right)\|\nabla I\|^2 - \left(\frac{1}{16}\right)(\nabla^2 I)^2\right|}{\left(I+\left(\frac{1}{4}\right)\nabla^2 I\right)^2}} \quad (5)$$

2.2 Proposed method

As shown in Fig. 1a, Yu and Acton [38] used a template of four closest neighbors of pixel (i, j) under analysis for calculation of derivative (∇I) and Laplacian $(\nabla^2 I)$ terms. These terms can be calculated more accurately by considering large-sized template of higher number of neighborhood pixels and the corresponding methodology improves the visual quality of speckled ultrasound imagery. In the proposed study, modified speckle reduction anisotropic diffusion methods are devised with three new templates of 12, 24, and 40 neighborhood pixels. As shown in Fig. 1b, the new template of 12 neighborhood pixels has a width of 5 pixels, therefore named template 5. Likewise the other two templates shown in Fig. 1c, d are named template 7 and template 9, respectively.

2.2.1 MSRAD method

MSRAD methodology is explained in this section. The time and space coordinates are discretized as

$$t = n\Delta t, \quad n = 0, 1, 2\ldots$$

$$x = ih, \quad i = 0,\ 1,\ 2\ldots, M-1$$

$$y = jh, \quad j = 0,\ 1,\ 2\ldots, N-1$$

$$I_{i,j}^{n} = I(ih, jh, n\Delta t)$$

where Δt is a time step size between two consecutive iterations and h is a spatial step size between two consecutive pixels in x and y directions on the image of the size $Mh \times Nh$. In numerical implementation, h is assumed as 1, thus I_{ij}^{n} represents the image pixel intensity at position (i, j) at time iteration n.

The discrete form of the instantaneous coefficient of variation ICOV_{ij}^{n} can be expressed in terms of spatial neighborhood of pixel (i, j) as

$$\mathrm{ICOV}_{i,j}^{n} = \sqrt{\frac{\left|\left(\frac{1}{2}\right)\left\|\nabla I_{i,j}^{n}\right\|^2 - \left(\frac{1}{|\eta_{i,j}|^2}\right)\left(\nabla^2 I_{i,j}^{n}\right)^2\right|}{\left(I_{i,j}^{n}+\left(\frac{1}{|\eta_{i,j}|}\right)\nabla^2 I_{i,j}^{n}\right)^2}} \quad (6)$$

Thus instantaneous coefficient of variation for template 5 is given by

$$\mathrm{ICOV}_{i,j}^{n} = \sqrt{\frac{\left|\left(\frac{1}{2}\right)\left\|\nabla I_{i,j}^{n}\right\|^2 - \left(\frac{1}{12^2}\right)\left(\nabla^2 I_{i,j}^{n}\right)^2\right|}{\left(I_{i,j}^{n}+\left(\frac{1}{12}\right)\nabla^2 I_{i,j}^{n}\right)^2}} \quad (7)$$

Figure 2 shows the neighborhood pixel representation of pixel (i, j) in template 5. To explain the derivative calculations by using template 5, pixels in template 5 are grouped on the basis of their distances from the central pixel. These groups are shown below:

First group: Pixels at a distance h from the center pixel are

$$I_{i-1,j}^{n}, I_{i,j-1}^{n}, I_{i+1,j}^{n} \text{ and } I_{i,j+1}^{n}$$

For these Pixels, derivative approximations can be calculated as

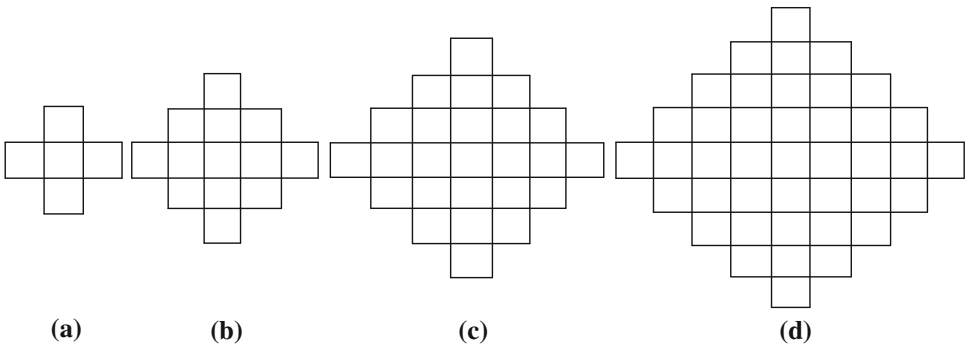

Fig. 1 Template of the pixel (i, j) **a** template used in the SRAD method, **b** template 5, **c** template 7 and **d** template 9 used in the proposed MSRAD method

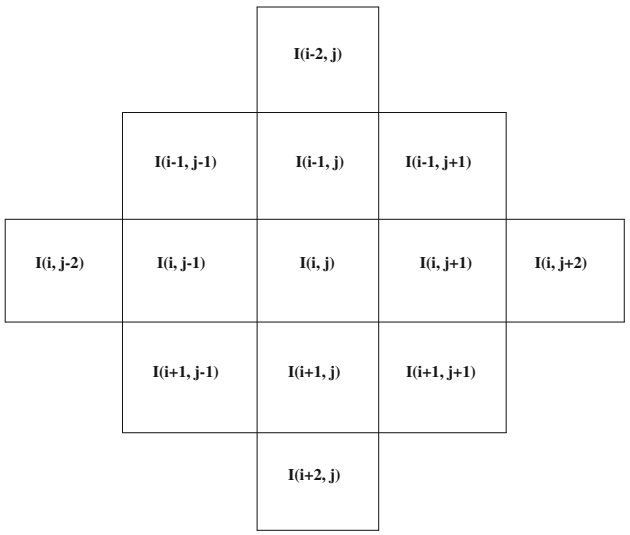

Fig. 2 Representation of pixel (i, j) and its neighborhood pixels in MSRAD-template 5

$$\frac{I^n_{i-1,j}-I^n_{i,j}}{h},\frac{I^n_{i,j-1}-I^n_{i,j}}{h},\frac{I^n_{i+1,j}-I^n_{i,j}}{h}\text{ and }\frac{I^n_{i,j+1}-I^n_{i,j}}{h}$$

and Laplacian approximations can be calculated as

$$\frac{I^n_{i-1,j}+I^n_{i,j-1}+I^n_{i+1,j}+I^n_{i,j+1}-4I^n_{i,j}}{h^2}$$

where, $h = 1$.

Second group: Pixels at a distance $\sqrt{2}h$ from the center pixel are

$$I^n_{i-1,j-1}, I^n_{i+1,j-1}, I^n_{i+1,j+1}\text{ and }I^n_{i-1,j+1}$$

For these Pixels derivative approximations can be calculated as

$$\frac{I^n_{i-1,j-1}-I^n_{i,j}}{\sqrt{2}h},\frac{I^n_{i+1,j-1}-I^n_{i,j}}{\sqrt{2}h},\frac{I^n_{i+1,j+1}-I^n_{i,j}}{\sqrt{2}h}\text{ and }\frac{I^n_{i-1,j+1}-I^n_{i,j}}{\sqrt{2}h}$$

and Laplacian approximations can be calculated as

$$\frac{I^n_{i-1,j-1}+I^n_{i+1,j-1}+I^n_{i+1,j+1}+I^n_{i-1,j+1}-4I^n_{i,j}}{2h^2}$$

Third group: Pixels at a distance 2 h from the center pixel, and these are

$$I^n_{i-2,j}, I^n_{i+2,j}, I^n_{i,j-2}\text{ and }I^n_{i,j+2}$$

For these Pixels derivative approximations can be calculated as

$$\frac{I^n_{i-2,j}-I^n_{i,j}}{2h},\frac{I^n_{i+2,j}-I^n_{i,j}}{2h},\frac{I^n_{i,j-2}-I^n_{i,j}}{2h}\text{ and }\frac{I^n_{i,j+2}-I^n_{i,j}}{2h}$$

and Laplacian approximations can be calculated as

$$\frac{I^n_{i-2,j}+I^n_{i+2,j}+I^n_{i,j-2}+I^n_{i,j+2}-4I^n_{i,j}}{4h^2}$$

The derivative approximations calculated in all the three groups are summed up and similarly the Laplacian approximations are also summed up. Finally, the diffusion coefficient is estimated as follows:

$$c\left(\mathrm{ICOV}^n_{i,j}\right)\equiv c^n_{i,j}=\frac{1}{1+\left(\left(\mathrm{ICOV}^n_{i,j}\right)^2-\mathrm{ICOV}_0(n)^2\Big/\mathrm{ICOV}_0(n)^2\left(1+\mathrm{ICOV}_0(n)^2\right)\right)} \tag{8}$$

where,

$$\mathrm{ICOV}_0(n)=\left(1.4826\Big/\sqrt{2}\right)\mathrm{MAD}(I(n))$$
$$=1.0484\ \mathrm{median}[\|I(n)-\mathrm{median}\{\|I(n)\|\}\|] \tag{9}$$

MAD denotes the median absolute deviation and the multiplying factor 1.4826 is derived from the fact that the

MAD of a zero-mean normal distribution with unit variance is 1/1.4826 [5, 39].

Divergence term is calculated in three parts according to these three groups of pixels.

$$d1^n_{i,j} = \frac{1}{h^2}\Big[c^n_{i+1,j}\Big(I^n_{i+1,j} - I^n_{i,j}\Big) + c^n_{i-1,j}\Big(I^n_{i-1,j} - I^n_{i,j}\Big) + c^n_{i,j-1}\Big(I^n_{i,j-1} - I^n_{i,j}\Big) + c^n_{i,j+1}\Big(I^n_{i,j+1} - I^n_{i,j}\Big)\Big]$$

$$d2^n_{i,j} = \frac{1}{2h^2}\Big[c^n_{i-1,j-1}\Big(I^n_{i-1,j-1} - I^n_{i,j}\Big) + c^n_{i+1,j-1}\Big(I^n_{i+1,j-1} - I^n_{i,j}\Big) + c^n_{i+1,j+1}\Big(I^n_{i+1,j+1} - I^n_{i,j}\Big) + c^n_{i-1,j+1}\Big(I^n_{i-1,j+1} - I^n_{i,j}\Big)\Big]$$

and

$$d3^n_{i,j} = \frac{1}{4h^2}\Big[c^n_{i-2,j}\Big(I^n_{i-2,j} - I^n_{i,j}\Big) + c^n_{i+2,j}\Big(I^n_{i+2,j} - I^n_{i,j}\Big) + c^n_{i,j-2}\Big(I^n_{i,j-2} - I^n_{i,j}\Big) + c^n_{i,j+2}\Big(I^n_{i,j+2} - I^n_{i,j}\Big)\Big].$$

Finally,

$$I^{n+1}_{i,j} = I^n_{i,j} + \frac{\Delta t}{12}\Big(d1^n_{i,j} + d2^n_{i,j} + d3^n_{i,j}\Big) \tag{10}$$

Similarly, ICOV^n_{ij} and I^{n+1}_{ij} with template 7 and template 9 are given as:

With template 7

$$\mathrm{ICOV}^n_{i,j} = \sqrt{\frac{\left|\left(\frac{1}{2}\right)\left\|\nabla I^n_{i,j}\right\|^2 - \left(\frac{1}{24^2}\right)\left(\nabla^2 I^n_{i,j}\right)^2\right|}{\left(I^n_{i,j} + \left(\frac{1}{24}\right)\nabla^2 I^n_{i,j}\right)^2}} \tag{11}$$

$$I^{n+1}_{i,j} = I^n_{i,j} + \frac{\Delta t}{24}\left(\sum_{P=1}^{6} dP^n_{i,j}\right) \tag{12}$$

With template 9

$$\mathrm{ICOV}^n_{i,j} = \sqrt{\frac{\left|\left(\frac{1}{2}\right)\left\|\nabla I^n_{i,j}\right\|^2 - \left(\frac{1}{40^2}\right)\left(\nabla^2 I^n_{i,j}\right)^2\right|}{\left(I^n_{i,j} + \left(\frac{1}{40}\right)\nabla^2 I^n_{i,j}\right)^2}} \tag{13}$$

$$I^{n+1}_{i,j} = I^n_{i,j} + \frac{\Delta t}{40}\left(\sum_{P=1}^{10} dP^n_{i,j}\right) \tag{14}$$

where each term of ∇I^n_{ij}, $\nabla^2 I^n_{ij}$, and dP^n_{ij} is calculated according to the template pixel distances from the central pixel (i, j).

2.2.2 Enhancement method

A regularized-SRAD [40] is a point-wise energy-condensation regulation technique that enhances the SRAD outputs with better preserving bright points, linear, and regional features. This technique comprised of two components: the SRAD diffusion component that retains the characteristics of SRAD speckle filtering, and the energy contraction component that enables the image to be more appealing to human visual systems. The discretized form of regularized-SRAD can be written as below:

$$I^{n+1}_{i,j} = I^n_{i,j} + \frac{\Delta t}{4}\Big(d^n_{i,j}\Big) - \lambda\gamma(\mathrm{Ic}^n)^{-\gamma}\Big(I^n_{i,j}\Big)^{\gamma-1} \tag{15}$$

where λ is a positive weight factor, γ is a parameter greater than unity, and Ic is a threshold value above which image features are considered bright. In the present study, regularization is added with MSRAD approximations and the discretized form of methods for each template are given below:

For regularized MSRAD-template 5,

$$I^{n+1}_{i,j} = I^n_{i,j} + \frac{\Delta t}{12}\left(\sum_{P=1}^{3} dP^n_{i,j}\right) - \lambda\gamma(\mathrm{Ic}^n)^{-\gamma}\Big(I^n_{i,j}\Big)^{\gamma-1}, \tag{16}$$

For regularized MSRAD-template 7,

$$I^{n+1}_{i,j} = I^n_{i,j} + \frac{\Delta t}{24}\left(\sum_{P=1}^{6} dP^n_{i,j}\right) - \lambda\gamma(\mathrm{Ic}^n)^{-\gamma}\Big(I^n_{i,j}\Big)^{\gamma-1}, \tag{17}$$

and for regularized MSRAD-template 9

$$I^{n+1}_{i,j} = I^n_{i,j} + \frac{\Delta t}{40}\left(\sum_{P=1}^{10} dP^n_{i,j}\right) - \lambda\gamma(\mathrm{Ic}^n)^{-\gamma}\Big(I^n_{i,j}\Big)^{\gamma-1}. \tag{18}$$

Mean of the processed images are preserved as the same as that of original image.

2.3 Aspects related to the tests with real images

Ultrasound images were acquired from the ATL HDI-5000 ultrasound scanner under the supervision of medical radiologists. The testing of proposed methodology was done by two ways: subjectively and objectively. First, the proposed modifications in SRAD were examined for the assessment of ultrasound image quality improvement via visual evaluation by the senior radiologists. Visual evaluation is defined as the ability of an expert radiologist to extract useful anatomical information from an ultrasound image. Visual evaluation varies from expert to expert and is subject to observer's variability. Visual evaluation of processed ultrasound images was assessed by two expert radiologists associated with an Institute of national repute; one of them is Professor & Head and the other is Associate Professor in the Department of Radiodiagnosis, Postgraduate Institute of Medical Education & Research, Chandigarh, India. The second performance assessment criterion is objective performance metrics to test the image

quality improvement of processed images using MSRAD methods in comparison to SRAD method.

2.3.1 Methodology to evaluate the performance subjectively

The subjective performance evaluation was carried out in two experiments:

Experiment 1 A dataset of 111 ultrasound liver images, comprising of 17 cyst, 15 Hepatocellular carcinomas (HCC), 18 Hemangiomas, 45 Metastases and 16 Normal liver images, were processed with SRAD and MSRAD-template 5 method. The processed images were shown to radiologists for subjective evaluation and they assessed improvement in all the 111 images. They also suggested that there is no need to consider normal images for further experiments with MSRAD-template 7 and -template 9, as there is no lesion information with the normal one. Therefore, only 95 lesion ultrasound images were processed with MSRAD-template 7 and -template 9 algorithms. For subjective evaluation by the radiologists, first, the original and the processed images were coded and each coded set of images was given to the expert radiologists in their separate chambers for marking unbiasedly the best image from the individual set. Four was the score that was assigned for the best processed image from the set of processed images for a particular liver image and zero was assigned for the worst one. One, two and three were the scores for images with intermediate results. Marked images were collected separately from both the experts. At the last, images were decoded and relative outcomes were tabulated as per the expert's opinion. Scores of both the radiologists were added as per the used processing method per image for final results to compare algorithms via visual evaluation

Experiment 2 In this second experiment, 95 lesion ultrasound images and their enhanced counterparts by regularized SRAD, regularized MSRAD-template 5, -template 7 and -template 9 methods were put before the experts for visual evaluation. For each case, original and the processed images were presented without labeling (coded as before) at random to the two experts. The experts were asked to assign a score according to low and high subjective visual perception criterion. Visual perception criterion is based on the quality of a processed image which can be said to be an enhanced version of the original image if it allows the observer to perceive better the desired information in the image. Visual scores (per enhancement method per image) of both the radiologists were obtained and added in the same way as mentioned in experiment 1. Finally, a comparative evaluation of methods was made with the final results

2.3.2 Performance measures to evaluate the method objectively

Objectively, the differences between the original, g_{ij} and the processed, f_{ij} images were evaluated using image quality evaluation metrics. The performance measures, which have clear physical meaning, were computed; they include beta-metric(β), correlation coefficient(ρ), Pratt's figure of merit (FOM) and universal image quality index (Q). These performance measures are given below:

(a) The performance of edge preservation is evaluated by beta metric (β) as used in [29, 45] and computed by

$$\text{beta metric} = \frac{D\left(\Delta g - \overline{\Delta g}, \Delta f - \overline{\Delta f}\right)}{\sqrt{D\left(\Delta g - \overline{\Delta g}, \Delta g - \overline{\Delta g}\right).D\left(\Delta f - \overline{\Delta f}, \Delta f - \overline{\Delta f}\right)}} \tag{19}$$

In the above expression, symbols Δg and Δf represent the high-pass filtered versions of g and f, respectively, calculated with a 3×3 pixel standard approximation of the Laplacian operator. $\overline{\Delta g}$ and $\overline{\Delta f}$ are mean intensity value of pixels in the region of Δg and Δf, respectively. Function D is defined as $D(s_1, s_2) = \sum_{i=1}^{M}\sum_{j=1}^{N} g_{ij} \cdot f_{ij}$. This quantitative performance measure should be close to unity for an optimal effect of edge preservation.

(b) The correlation coefficient (ρ) between the original and processed images of size $M \times N$ is defined by the expression as given below [32]

$$\rho = \frac{\sum_{i=1}^{M}\sum_{j=1}^{N} g_{ij} \cdot f_{ij}}{\sqrt{\sum_{i=1}^{M}\sum_{j=1}^{N} g_{ij}^2}\sqrt{\sum_{i=1}^{M}\sum_{j=1}^{N} f_{ij}^2}} \tag{20}$$

(c) The Pratt's Figure of Merit (FOM) is defined as given below [25, 38]

$$\mathrm{FOM} = \frac{1}{\max\{\hat{N}, N_{\mathrm{ideal}}\}} \sum_{i=1}^{\hat{N}} \frac{1}{1 + d_i^2 \alpha} \tag{21}$$

where $\hat{N}$ and N_{ideal} are the number of detected and ideal edge pixels, respectively, d_i is the Euclidean distance between the ith detected edge pixel and the nearest ideal edge pixel, and α is a constant typically set to 1/9. FOM ranges between 0 and 1, with unity for ideal edge detection. The Canny edge detector is used to find the edge in all processed results with a standard deviation of 0.1 and a threshold of 0.5 [18, 38].

(d) The universal image quality index (Q) which measures the distortion between two images, modeled as a combination of three factors, the loss of correlation, luminance distortion and contrast distortion. It is expressed as [21, 33]

$$Q = \frac{\sigma_{gf}}{\sigma_f \sigma_g} \cdot \frac{2\overline{f}\,\overline{g}}{(\overline{f})^2 + (\overline{g})^2} \cdot \frac{2\sigma_f \sigma_g}{\sigma_f^2 + \sigma_g^2}, \quad -1 \langle Q \langle 1 \tag{22}$$

where $\overline{g}$ and $\overline{f}$ represent the mean of the original and filtered images with their standard deviations, σ_g and σ_f, of the original and despeckled values of the analysis window, and σ_{gf} represents the covariance between the original and filtered windows. Q is computed as an average of all Q values at each pixel. The local Q value for each pixel is calculated for a sliding window of 8×8 without overlapping. The dynamic range of Q is between -1 and 1, the best value of $Q = 1$ is achieved if and only if the two images are equal. Higher the Q values, the less will be the distortion between the original and the processed image.

3 Results

The proposed MSRAD methods and their regularized forms are tested with 111 ultrasound images of normal liver and liver with focal diseases. Methods are evaluated subjectively by the expert radiologist and objectively by the image quality performance measures. The results of subjective evaluation in experiment 1 are given below:

(i) Out of 95 lesion ultrasound images, 84 images that are processed images by MSRAD-template 9 method got the highest visual score, i.e., four in comparison to original and other processed images.

(ii) Out of 15 cases of HCC, visual scores of 6 cases are the same for the original and processed images by MSRAD-template 9. For these cases, radiologists say that it is difficult to observe an improvement by MSRAD-template 9 over the original image on the basis of visual evaluation only.

(iii) Figure 3 shows original and processed images of Cyst, Metastasis and Hemangioma. Lesion is indicated by the region marked by arrows in original images A1, A2, and A3. Image texture in images C1, C2, and C3 (processed by MSRAD-template 5) is better visualized than that in images B1, B2, and B3 (processed by SRAD), respectively. Texture preservation increases with MSRAD-template 7 and texture looks like the original one with the application of MSRAD-template 9 method. Finally, MSRAD-template 9 processed images (E1, E2, and E3) give better visual appearance in comparison to the original ones with slightly enhance texture contrast and reduced blurring. All these visual comparisons between original and processed images can be observed in the marked bounded regions of Fig. 3.

Subjective findings of MSRAD methods are supported by objective image quality measures. Table 1 summarizes the comparison of SRAD and MSRAD filtering methods based on the values of objective measures. These measures are calculated for each 111 ultrasound images to reduce the sample bias and their values are listed in Table 1 with their mean and standard deviation. Mean value of β is 0.7064 for SRAD, 0.9302 for MSRAD-template 5 and it increases up to 0.9987 for MSRAD-template 9. Value of correlation coefficient (ρ) is improved with MSRAD methods in comparison to SRAD. FOM is improved from 0.63 for SRAD to 0.84 $\sim$ 0.99 for MSRAD methods. Finally, universal image quality index,Q, is also improved with MSRAD methods. It is observed from Table 1 that the values of all objective parameters are the highest for MSRAD-template 9.

For better resolution of point and linear features, regularization is incorporated with MSRAD in the similar fashion as used by Yu and Yadegar [40] with SRAD method. The following value of the parameters or choices are used for satisfactory results in application on ultrasound images with focal liver diseases; (1) weight $\lambda = 0.0005$; (2) gamma $\gamma = 2.0$ and 3) $\mathrm{Ic}^n = \mathrm{median}(I^n)$. Stability of numerical approximation in partial differential equation depends on the value of time step size Δt. Lower bound for Δt value is greater than zero and upper bound is 0.1428, 0.11 and 0.089 for template 5, template 7 or template 9, respectively. Therefore, Δt is taken as 0.05 to assure the stability in diffusion process. A threshold value of 0.01 of MSE was chosen as a stopping criterion for diffusion process. When, the proposed methods were applied to several images, the convergence is achieved in iterations ranging 80–110. Therefore, for the sake of comparison among the proposed methods, a common value of iteration, i.e., $n = 120$, was considered as a stopping criterion. Processed methods are implemented in MATLAB (Mathworks, Natick, MA), version 7.5 and achieved a

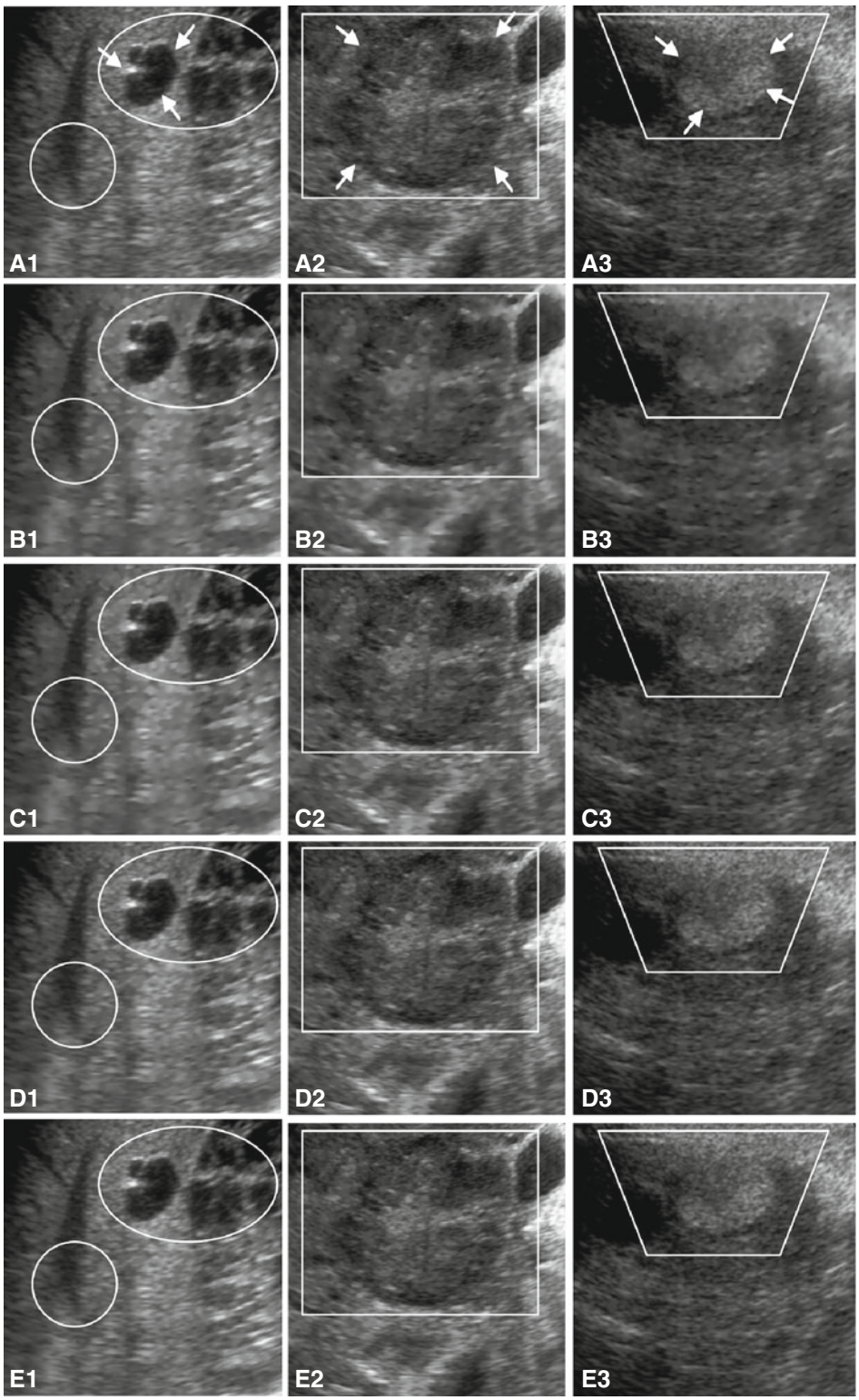

A: Original image
B: Processed image by SRAD
C: Processed image by MSRAD-template5
D: Processed image by MSRAD template7
E: Processed image by MSRAD-template9

1: Cyst
2: Metastasis
3: Hemangioma

Fig. 3 Original and processed images by SRAD and proposed methods

Table 1 Performance comparison of the filtering Methods

Performance measures	SRAD	MSRAD-template 5	MSRAD-template 7	MSRAD-template 9
β	$0.7064 \pm 7.88 \times 10^{-2}$	$0.9302 \pm 3.80 \times 10^{-2}$	$0.9924 \pm 5.36 \times 10^{-3}$	$0.9987 \pm 9.70 \times 10^{-4}$
ρ	$0.99644 \pm 9.23 \times 10^{-4}$	$0.99920 \pm 3.93 \times 10^{-4}$	$0.99990 \pm 6.41 \times 10^{-5}$	$0.99999 \pm 1.14 \times 10^{-5}$
FOM	0.63 ± 0.10	0.84 ± 0.07	0.95 ± 0.03	0.99 ± 0.01
Q	$0.99201 \pm 2.04 \times 10^{-3}$	$0.99824 \pm 8.48 \times 10^{-4}$	$0.99979 \pm 1.37 \times 10^{-4}$	$0.99997 \pm 2.4338 \times 10^{-5}$

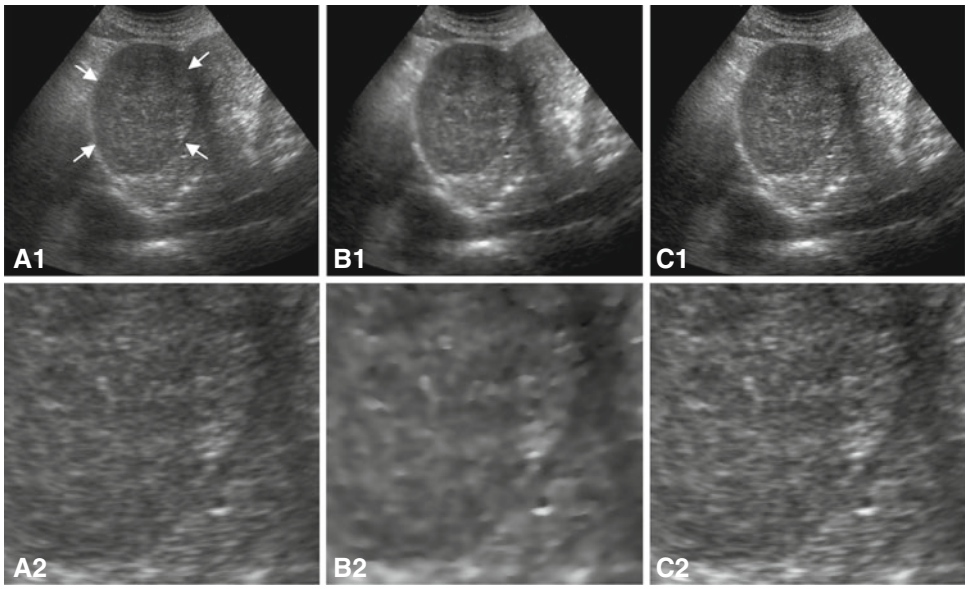

Fig. 4 Original and processed images by regularized SRAD and regularized MSRAD-template 9 method

A: Original image
B: Processed image by SRAD
C: Processed image by MSRAD-template9

1: HCC lesion
2: Close-up of area near lesion boundary

processing rate 0.32, 0.55, 0.98 s/iteration with regularized MSRAD-template 5, -template 7 and -template 9, respectively, for a 128 × 128 image on a PC with a Pentium 4 (1.7 GHz) processor. The scores of subjective evaluation in experiment 2 are the highest with regularized MSRAD-template 9 method for all the images. Figure 4 demonstrate the results with the original HCC image in A1 where HCC lesion is marked by arrows. Regularized SRAD processed image is indicated as B1 and regularized MSRAD-template 9 processed image is indicated as C1. The images A2, B2, and C2 represent the close up of area near lesion boundary of images A1, B1, and C1, respectively. It can be seen by the Fig. 4, that regularized MSRAD-template 9 processed image perceptibly enhances the texture of the image, whereas regularized SRAD processed image gives only intensity information rather than texture information.

4 Discussion

Since the lesions may have low contrast with adjacent host organs in conventional ultrasonic images, the objective of present study is to develop a controlled speckle reduction technique, with the help of radiologists' interpretation for enhancement of ultrasound image texture so that lesion can be easily detected. To achieve this objective, SRAD algorithm is modified, on the basis of radiologist's interpretations, to enhance the medical details of the liver ultrasound images. Modifications include the application of large-sized templates for calculation of diffusion, derivative, and Laplacian terms and finally regularization is incorporated for increasing the resolution of details in ultrasound images.

Visual study of the processed images by SRAD method shows that speckles are reduced at the cost of appearance of the image textures. Radiologists assessed that SRAD method is satisfactory for moderate and large size of cyst detection, but not suited for the disease detection such as HCC, Hemangioma and Metastasis. Thus, images processed by SRAD method are considered suitable where echogenicity is a main criterion for lesion detection; for example typical images of the cyst. SRAD processed images are not acceptable in the cases of (1) detection of cyst of small size, (2) atypical cases of cyst and (3) lesions

where image texture is a parameter to detect the lesion. HCC, Hemangioma, Metastasis and Normal liver are mainly identified by visualizing their texture. Speckle formation in ultrasound image is an integral part of image texture. Ultrasound image interpretation by the experienced radiologists wants the removal of speckle up to a level that hidden information behind it should not be affected and blurring of image details should be reduced for overall improvement in image visual quality. Therefore, the first necessity of texture enhancement is texture preservation. Keeping this fact in mind, SRAD method is modified with radiologist interpretation and resulted in MSRAD methods.

It is observed that the improvement in visual quality of processed images by MSRAD method increases as template size increases. Out of these proposed templates, application of template 9 gives best processed image in terms of reduction of blurring with slight enhancement of features. It is also approved by the expert radiologists that the application of template 9 gives processed images with best preservation of texture.

Results of subjective evaluation methodology are supported by the objective image quality performance measures and the values of these performance measures are listed in Table 1. β and FOM are edge preservation indices and their values show that the results are best with MSRAD-template 9. Higher values of β and FOM with MSRAD methods indicates better visualization due to edge preservation and hence suggest that MSRAD methods outperform SRAD in terms of edge preservation. High values of correlation measure, ρ, for MSRAD methods show that MSRAD processed images are quite similar to the original one in the sense that the image textures in the processed image are preserved. The overall improvement of image quality with MSRAD methods are supported by the high value of Universal image quality index, Q. Best values of all the measures with MSRAD-template 9 and the results of subjective evaluation support the choice of this template method.

MSRAD with regularization increases the effectiveness of method in terms of contrast enhancement. As compared to MSRAD methods, the regularized MSRAD methods give better results for diagnostic interpretations. After the final evaluation, the results of regularized MSRAD-template 9 were appreciated by the radiologists.

Finally, it is concluded that the proposed MSRAD method reduces speckle without blurring the image and increases the contrast of image texture that allows the fine details of image to be visualized clearly. The performance of MSRAD method is tested on a large data set and evaluated by medical experts both objectively and subjectively.

Acknowledgments The authors wish to acknowledge the Department of Electrical Engineering, Indian Institute of Technology Roorkee, Roorkee and the Department of Radiodiagnosis and Imaging, Postgraduate Institute of Medical Education and Research, Chandigarh for their constant patronage and support in carrying out the research work.

References

1. Abbott JG, Thurstone FL (1979) Acoustic speckle: theory and experimental analysis. Ultrason Imaging 1:303–324
2. Abd-Elmoniem KZ, Kadah YM, Youssef AM (2000) Real time adaptive ultrasound speckle reduction and coherence enhancement. In: International conference on image processing. Vancouver, Canada
3. Abd-Elmoniem KZ, Youssef A-BM, Kadah YM (2002) Real-time speckle reduction and coherence enhancement in ultrasound imaging via nonlinear anisotropic diffusion. IEEE Trans Biomed Eng 49(9):997–1014
4. Acton ST (2005) Deconvolutional speckle reducing anisotropic diffusion. In: Proceedings of the IEEE international conference on image processing. Charlottesville, USA
5. Aja-Fernandez S, Alberola-Lopez C (2006) On the estimation of the coefficient of variation for anisotropic diffusion speckle filtering. IEEE Trans Image Process 15(9):2694–2701
6. Badawi AM (2007) Scatterer density in nonlinear diffusion for speckle reduction in ultrasound imaging: the isotropic case. Int J Biol Biomed Med Sci 3:149–167
7. Badawi AM, Rushdi MA (2006) Speckle reduction in medical ultrasound: a novel scatterer density weighted nonlinear diffusion algorithm implemented as a neural-network filter. In: Proceedings of the IEEE international conference on engineering in medicine and biology society. New York, USA
8. Binh NT, Thanh NC (2007) Object detection of speckle image base on curvelet transform. ARPN J Eng Appl Sci 2(3):14–16
9. Black MJ, Sapiro G, Marimont DH, Hegger D (1998) Robust anisotropic diffusion. IEEE Trans Image Process 7(3):421–432
10. Brownrigg DRK (1984) The weighted median filter. Commun Assoc Comput Mach 27:204–208
11. Chen Y, Yin R, Flynn P, Broschat S (2003) Aggressive region growing for speckle reduction in ultrasound images. Pattern Recogn Lett 24:677–691
12. Frost VS, Stiles JA, Shanmugan KS, Holtzman JC (1982) A model for radar images and its application to adaptive digital filtering of multiplicative noise. IEEE Trans Pattern Anal Mach Intell PAMI-4: 157–165
13. Gerig G, Kubler O, Kikinis R, Jolesz FA (1992) Nonlinear anisotropic filtering of MRI data. IEEE Trans Med Imaging 11(2):221–232
14. Gupta S, Chauhan RC, Sexana SC (2004) Wavelet-based statistical approach for speckle reduction in medical ultrasound images. Med Bio Eng Comput 42(2):189–192
15. Kim YS, Ra JB (2005) Improvement of ultrasound image based on wavelet transform: speckle reduction and edge enhancement. In: Proceedings of SPIE, vol 5747. Bellingham, WA
16. Kim HS, Yoo JM, Park MS, Dinh TN, Lee GS (2007) An anisotropic diffusion based on diagonal edges. In: the 9th international conference on advanced communication technology, pp 384–388
17. Kim HS, Yoon HS, Toan ND, Lee GS (2008) Anisotropic diffusion transform based on directions of edges. In: Proceedings of the IEEE international conference on computer and information technology workshops. Washington, USA, pp 386–400
18. Krissian K, Westin C-F, Kikinis R, Vosburgh KG (2007) Oriented speckle reducing anisotropic diffusion. IEEE Trans Image Process 16(5):1412–1424

19. Kuan DT, Sawchuk AA, Strand TC, Chavel P (1987) Adaptive restoration of image with speckle. IEEE Trans Acoust Speech Signal Process ASSP 35:373–383
20. Lee JS (1986) Speckle suppression and analysis for synthetic aperture radar. Opt Eng 25:636–643
21. Loizou CP, Pattichis CS, Pantziaris M, Tyllis T, Nicolaides A (2006) Quality evaluation of ultrasound imaging in the carotid artery based on normalization and speckle reduction filtering. Med Biol Eng Comput 44(5):414–426
22. Ma J, Plonka G (2007) Combined curvelet shrinkage and nonlinear anisotropic diffusion. IEEE Trans Image Process 16(9): 2198–2206
23. Maalouf A, Carré P, Augereau B, Fernandez-Maloigne C (2007) Bandelet-based anisotropic diffusion. In: Proceedings of the IEEE international conference on image processing, pp 289-292
24. Perona P, Malik J (1990) Scale space and edge detection using anisotropic diffusion. IEEE Trans Pattern Anal Mach Intell 12:629–639
25. Pratt WK (1977) Digital image processing. Wiley, New York
26. Rabbani H, Vafadust M, Abolmaesumi P, Gazor S (2008) Speckle noise reduction of medical ultrasound images in complex wavelet domain using mixture priors. IEEE Trans Biomed Eng 55(9):2152–2160
27. Rajan J, Kaimal MR (2006) Image denoising using wavelet embedded anisotropic diffusion (WEAD). In: Proceedings of the IEEE international conference on visual information engineering, pp 589–593
28. Saad AS (2006) Speckle reduction of ultrasound images using wavelets analysis. IMIBE, Germany, pp 51–54
29. Sattar F, Floreby L, Salomonsson G, Lovstrom B (1997) Image enhancement based on a nonlinear multiscale method. IEEE Trans Image Process 6(6):888–895
30. Song X-Y, Zhang S, Song K-O, Yang W, Chen Y-Z (2008) Speckle supression for medical ultrasound images based on modelling speckle with rayleigh distribution in contourlet domain. In: Proceedings of the international conference on wavelet analysis and pattern recognition. Hong Kong, pp 194–199
31. Tauber C, Batatia H, Ayache A (2004) A robust speckle reduction anisotropic diffusion. In: Proceedings of the IEEE international conference on image processing, pp 247–250
32. Thakur A, Anand R (2005) Image quality based comparative evaluation of wavelet filters in ultrasound speckle reduction. Dig Sig Process 15(5):455–465
33. Wang Z, Bovik A (2002) A universal quality index. IEEE Signal Proc Lett 9(3):81–84
34. Wang B, Liu DC (2008) A novel edge enhancement method for ultrasound imaging. In: Proceedings of the IEEE international conference on bioinformatics, biomedical engineering. Shanghai, China, pp 2414–2417
35. Weickert J (1997) A review of nonlinear diffusion filtering. In: ter Haar Romeny BM, Florack L, Koederink J, Viergever M (eds) Lecture notes in computer science, scale-space theory in computer vision, vol 1252. Springer-Verlag, Germany; Berlin, pp 3–28
36. Xie J, Jiang YF, Tsui HT, Heng PA (2006) Boundary enhancement and speckle reduction for ultrasound images via salient structure extraction. IEEE Trans Biomed Eng 53:2300–2309
37. Yang Z, Fox MD (2004) Speckle reduction and structure enhancement by multichannel median boosted anisotropic diffusion. EURASIP J App Sig Process 16:2492–2502
38. Yu Y, Acton ST (2002) Speckle reducing anisotropic diffusion. IEEE Trans Image Process 11:1260–1270
39. Yu Y, Acton ST (2004) Edge detection in ultrasound imagery using the instantaneous coefficient of variation. IEEE Trans Image Process 13(12):1640–1655
40. Yu Y, Yadegar J (2006) Regularized speckle reducing anisotropic diffusion for feature characterization. In: Proceedings of the IEEE international conference on image processing. CA: Los Angeles, pp 1577–1580
41. Yu Y, Molloy JA, Acton ST (2004) Generalized speckle reducing anisotropic diffusion for ultrasound imagery. In: Proceedings of the 17th IEEE symposium on computer-based medical system. Bethesda, Maryland, pp 279–284
42. Yue Y, Croitoru MM, Bidani A, Zwischenberger JB, Clark JW (2005) Ultrasound speckle suppression and edge enhancement using multiscale nonlinear wavelet diffusion. In: Proceedings of the IEEE international conference on engineering in medicine and biology society. Shanghai, China, pp 6429–6432
43. Yue Y, Croitoru MM, Bidani A, Zwischenberger JB, Clark JW (2006) Nonlinear multiscale wavelet diffusion for speckle suppression and edge enhancement in ultrasound images. IEEE Trans Med Imaging 25(3):297–311
44. Zhang F, Yoo YM, Zhang L, Koh LM, Kim Y (2006) Multiscale nonlinear diffusion and shock filter for ultrasound image enhancement. In: Proceedings of the 2006 IEEE computer society conference on computer vision and pattern recognition, pp 1972–1977
45. Zhang F, Yoo YM, Koh LM, Kim Y (2007) Nonlinear diffusion in Laplacian pyramid domain for ultrasonic speckle reduction. IEEE Trans Med Imaging 26(2):200–211